Frontiers in Bioscience Landmark

Front. Biosci. (Landmark Ed) **2025**; 30(12): 47370
https://doi.org/10.31083/FBL47370

Original Research

Role of the Longest Arm of Phycobilisome Core-Membrane Linker in Assembling the Phycobilisomes From *Synechocystis* sp. PCC 6803

Nannan Niu[1,*], Ning Chen[1], Huanhuan Feng[1], Xueli Du[1]

[1]Depatment of Medicine, Luoyang Polytechnic, 471000 Luoyang, Henan, China
*Correspondence: 847037660@qq.com (Nannan Niu)
Academic Editor: Graham Pawelec
Submitted: 15 October 2025 Revised: 30 November 2025 Accepted: 9 December 2025 Published: 22 December 2025

Abstract

Background: The phycobilisomes (PBS) of cyanobacteria and red algae are unique light-harvesting protein-pigment complexes that utilize bilin derivatives for light absorption and energy transfer. These extramembranous mega-Dalton complexes are specifically organized and anchored to photosystem II (PSII) via the multi-domain core-membrane linker (L_{CM}). While Arm2 is the longest segment in L_{CM} domain, its specific functions remain uncharacterized. **Methods**: A series of *Synechocystis* sp. PCC 6803 mutants with complete or partial deletions of Arm2 and its adjacent Rep domains within L_{CM} were constructed. The assembled PBSs were isolatedand characterized using sucrose gradient ultracentrifugation, absorption and fluorescence spectroscopy, and SDS-PAGE. Physiological functions were further assessed by analyzing growth, photosynthetic performance, state transitions, and non-photochemical quenching (NPQ). **Results**: Our results reveal that the super-secondary element of helix-turn-helix of Arm2 is critical for assembling the two longitudinal halves of PBS. The truncation of either or both helices of Arm2 results in the specific degradation of the longitudinal half harboring the terminal emitter, ApcD. Consequently, these mutants were deficient in state transitions and exhibited accelerated recovery from orange carotenoid protein (OCP)-mediated NPQ. We also identified the Arm2(37–67) motif likely involved in attaching the rods to the core, whereas the Arm2(68–129) region had no significant impact on PBS assembly. **Conclusions**: The helix-loop-helix element of Arm2 is essential for the longitudinal integrity of the PBS core and is a prerequisite for state transitions. These results suggest that state transitions may involve longitudinal rearrangements within the PBS structure, rather than lateral movements of the two halves, implicating that state transitions result from the longitudinal instead of the lateral moves of the two halves of the PBSs.

Keywords: *Synechocystis*; allophycocyanin; phycocyanin; linker; energy transfer; photoprotection

1. Introduction

Phycobilisomes (PBSs) are mega-Dalton light-harvesting complexes in cyanobacteria and red algae, composed of dozens of phycobiliproteins that organize hundreds of bilin chromophores [1]. These complexes absorb light across a broad spectrum (480–660 nm) and efficiently channel the energy to the photosynthetic reaction centers. This transfer occurs either directly or assisted by the chlorophylls (Chls) in the photosystems' core complexes [2,3]. Final energy delivery is facilitated by two terminal emitters containing phycocyanobilin (PCB): allophycocyanin (APC) B (AP-B) and the core-membrane linker (L_{CM}) [4,5].

L_{CM} is encoded by *apcE* gene and comprises an N-terminal PCB-binding domain (ApcEΔ) [4] and several C-terminal repeat (Rep) domains connected by three arm-loop domains [6]. In the *Synechocystis* sp. PCC6803 (hereby referred to as *Synechocystis*), the L_{CM} starts from the N-terminal ApcEΔ, followed by three successive Rep domains [Rep1(230–435 amino acid (aa)), Rep2(436–664 aa), Rep3(685–885 aa)] [7]. The precise role of L_{CM} assembles the PBS remains to be fully elucidated. According to the structure studies of L_{CM} in the red alga *Griffithsia pacifica* [8], Rep1 and Rep2 are located at the center of the two hexamer of Cylinder 1 (a basal cylinders of the PBS cores), connecting the two APC trimers of a hexamer, respectively, while Rep3 is localized in the central cavity of the hexamer of the top Cylinder 3 [8–10]. Although the disparities observed in the L_{CM} topology between actual red algae and modeled cyanobacteria could mirror genuine structural disparities, the high sequence homology shared by the L_{CM}s of both red algae and cyanobacteria hints at a comparable topological configuration within these two types of PBS [11]. This homology enabled Liu *et al.* [12] to contruct a validated structural model of the PBS in *Synechocystis* sp. PCC6803. This model was subsequently validated through rigorous chemical cross-linking analysis [12]. Electron microscopy [7,8] revealed that the cylinders are organized as a triangular prism with Cylinder 1 and 2 forming a base that lies on the top of the membrane and Cylinder 3 on the top of the base.

The connecting loops of *Synechocystis*' L_{CM} include Arm1(241–249) that connects Rep1(250–400) to the PCB-binding domain (ApcEΔ), Arm3(686–714) that connects Rep2(536–685) and Rep3(715–860) [13], and Arm2 (401–534) that connects Rep1 and Rep2. The Rep domains, which are ~120 amino acids long and share high similarity with pfam_00427 (the conserved domain of the rod linker

Copyright: © 2025 The Author(s). Published by IMR Press.
This is an open access article under the CC BY 4.0 license.

Publisher's Note: IMR Press stays neutral with regard to jurisdictional claims in published maps and institutional affiliations.

in PBS), play a vital role in fastening the APC discs [8]. Compared to the short Arm1 (9 aa) and Arm3 (29 aa), Arm2 is 134 aa in *Synechocystis* and effectuates like a functional domain. In *Griffithsia pacifica*, Arm2 consists of a super-secondary structure of helix-loop-helix followed by an unstructured extension [8], which is to the sequence in *Synechocystis* (**Supplementary Fig. 1**). Despite its prominence, the potential roles of Arm2 in PBSs are unknown.

In this study, we investigated the role of Arm2 in PBS assembly. We constructed a series of *Synechocystis* mutants with complete or partial truncation of Arm2 and/or deletions of its adjacent Rep2/Rep3 domains. Analysis of isolated PBSs, we found that the truncation of either one or both helices of Arm2 in L_{CM} split the PBSs longitudinally into a simple PBS consisting of the APC core and cyanobacterial phycocyanin (CPC) rod. Mutants with the damaged helix-loop-helix element of Arm2 were deficient in state transitions and exhibited accelerated recovery from non-photochemical quenching (NPQ) compared to wild-type (WT) and Rep3-truncated *Synechocystis* (Δ(*rep3*)).

2. Materials and Methods

2.1 Strains and Culture

Synechocystis and its mutants were grown in BG-11 medium on a shaker (130 rpm) at 30 °C under continuous white light (20 µmol photons $m^{-2}s^{-1}$ for LL) [14]. BG-11 medium with 1.2% (w/v) agar containing 0.3% (w/v) sodium thiosulfate was solidified for plate cultures. The photomixotrophic growth was achieved by diluting an aliquot from a photoautotrophic culture in the log phase (OD_{730} ~1.0) to an OD_{730} ~0.05 with BG-11 containing 10 mM glucose. The growth and cell densities were monitored at OD_{730} on a Beckman DU800 spectrophotometer. The growth was evaluated based on the average of three parallel experiments. Chlorophyll a (Chl *a*) [15] or phycocyanin (PC) [16] concentrations were determined by absorption spectroscopy and calculated per cell [17].

2.2 Cloning and Mutant Construction

All genetic manipulations were carried out according to standard protocols [18]. The *apcE* gene locus (*slr0335*) in *Synechocystis* encodes the L_{CM} protein, which consists the following domains: the N-terminal loop(80–150), Arm1(241–249), Rep1(250–400), Arm2(401–534), Rep2(535–685), Arm3(686–714), and Rep3(715–860). To delete these domains and/or motifs, mutation plasmids were constructed as follows.

2.2.1 Plasmid for Construction of Δ(rep3)

A 0.8-kbp DNA fragment including *arm2-rep2* and a 0.6-kbp DNA fragment including *arm3-rep3* of *apcE* was amplified from *Synechocystis* genomic DNA by PCR using primers P1–P4 (**Supplementary Table 1**), as upstream and downstream targeting arms, respectively. The restriction sites *Xho*I plus *Eco*RV and *Eco*RV plus *Xba*I were introduced in the targeting arms, respectively, for cloning the fragment into pBluescript. A DNA fragment containing streptomycin resistance cassette was excised from plasmid pHB45 via the restriction site *Sma*I and then inserted in the plasmid containing the targeting arms via the restriction site *Eco*RV, thereby yielding pBlue-Δ*(rep3)-str* (Fig. 1C, Ref. [19]).

2.2.2 Plasmid for Construction of Δ(arm2/rep3), Δ(rep2/rep3) and Δ(arm2/rep2/rep3)

A 1.7-kbp DNA fragment including *apcE*Δ*-arm1-rep1-*Δ*arm2-rep2* and a 0.6-kbp DNA fragment including arm3-rep3 was amplified from *Synechocystis* genomic DNA by PCR using primers P5-P10 (**Supplementary Table 1**) as upstream and downstream targeting arms, respectively. In the targeting arms, restriction sites of XhoI plus BamHI and BamHI plus XbaI were introduced to facilitate cloning of the targeting arms into pBluescript. A DNA fragment containing streptomycin resistance cassette was excised from plasmid pHB45(omega) via the restriction site BamHI and then inserted in the plasmid containing the targeting arms via the restriction site BamHI, yielding pBlue-Δ*(arm2/rep3)*-str (Fig. 1D). Similar strategies were employed for Δ*(rep2/rep3)* andΔ*(arm2/rep2/rep3)* using the primers listed in **Supplementary Table 1**.

2.2.3 Mutants Plasmids for Construction of Partially Arm2-Truncated Mutants Base on Δ(rep3)

A 5.3-kbp DNA fragment, including *pBlue-apcE*Δ*(arm2(6–36)/rep3)*, *pBlue-apcE*Δ*(arm2(37–67)/rep3)*, *pBlue-apcE*Δ*(arm2(68–98)/rep3)*, *pBlue-apcE*Δ*(arm2(99–129)/rep3)*, *pBlue-apcE*Δ*(arm2(6–17)/rep3)*, *pBlue-apcE*Δ*(arm2(18–28)/rep3)*, and *pBlue-apcE*Δ*(arm2(29–36)/rep3)*, was amplified from the plasmid of *pBlue-*Δ*(rep3)* by PCR using P17–P30 primers (**Supplementary Table 1**). Then, these plasmids were obtained by phosphorylation reaction and standard protocols, respectively. A DNA fragment containing streptomycin resistance cassette [4] was cut from plasmid pHB45(omega) via the restriction site BamHI and then inserted in the plasmid containing the targeting arms via the restriction site BamHI, yielding pBlue-Δ*(arm2(6–36)/rep3)*-str, pBlue-Δ*(arm2(37–67)/rep3)*-str, pBlue-Δ*(arm2(68–98)/rep3)*-str, pBlue-Δ*(arm2(99–129)/rep3)*-str, pBlue-Δ*(arm2(6–17)/rep3)*-str, pBlue-Δ*(arm2(18–28)/rep3)*-str, and pBlue-Δ*(arm2(29–36)/rep3)*-str.

2.3 Mutation of Synechocystis and Genetic Analyses

The mutant strains were generated by transforming WT Synechocytis cells with the respective plasmids via homologous recombination [20]. Transformants were selected on BG-11 plates containing 12.5 µg/mL spectinomycin, with segregation ensured throughsuccessive rounds of selection at 25 µg/mL spectinomycin. The genotypes of all final mutant strains were confirmed by PCR using re-

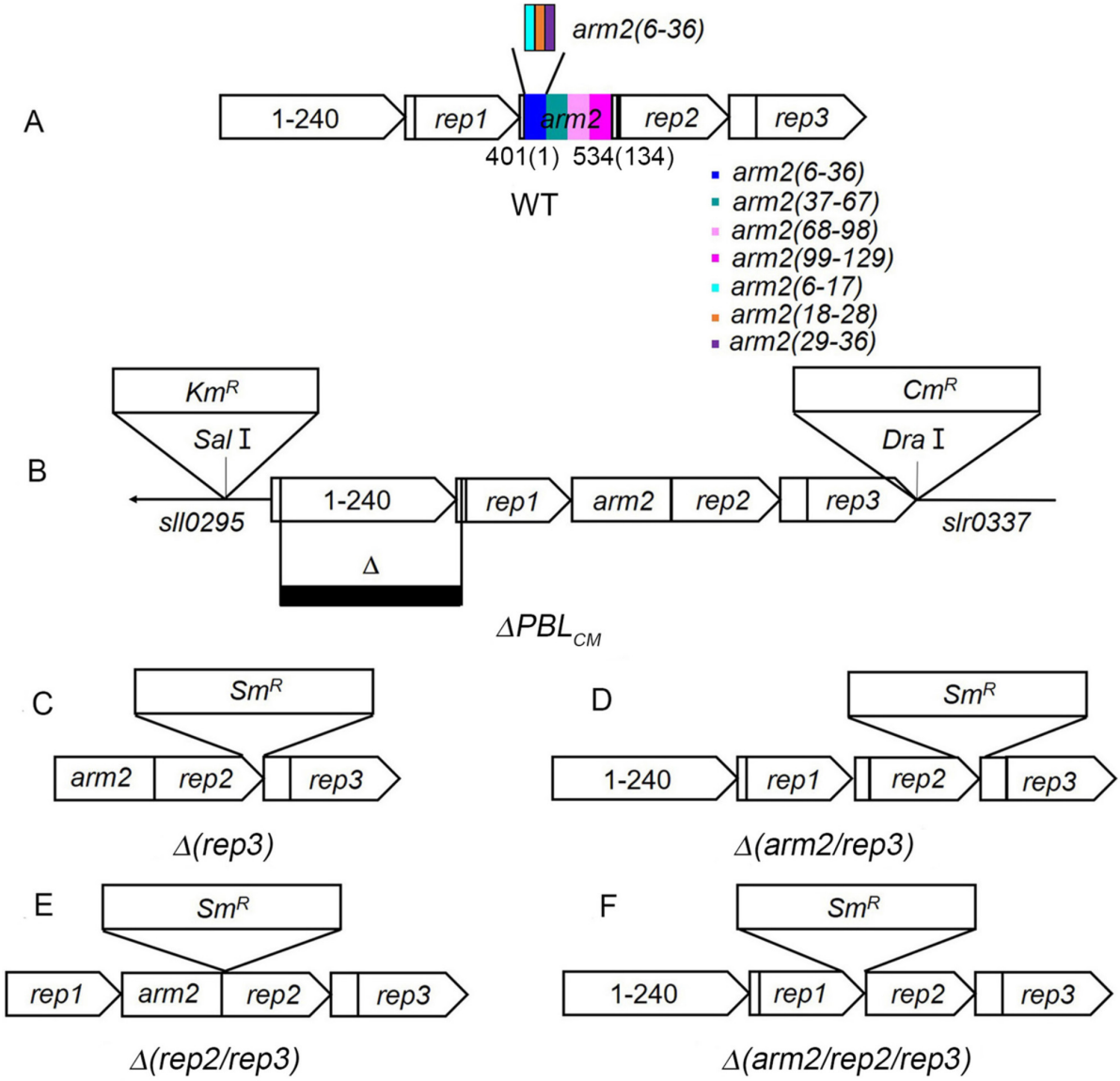

Fig. 1. Construction and characterization of ApcE-mutants in *Synechocystis* PCC 6803. (A) is the domain location in the ApcE protein and (B) is the Δ*PBL*$_{CM}$ mutant strain reported recently (Zlenko *et al*., 2019 [19]). In Δ(*rep3*) (C) Rep3 is deleted, in Δ(*arm2/rep3*) (D) Arm2 and Rep3 are deleted, in Δ(*rep2/rep3*) (E) Rep2 and Rep3 are deleted, in Δ(arm2/*rep2/rep3*) (F) Arm2, Rep2 and Rep3 are deleted from L$_{CM}$ of *Synechocystis* by inserting the spectinomycin resistance cassette. The other Arm2-truncated mutants were constructed based on Δ(*rep3*), and some amino acids deleted from Arm2 are shown in (A). Km^R stands for kanamycin resistance cassette, Cm^R indicates chloramphenicol resistance cassette, and Sm^R is spectinomycin resistance cassette.

spective primer sets (**Supplementary Fig. 2**, **Supplementary Table 1**).

2.4 Absorption Spectra and Sample Concentrations

The room temperature absorption spectra of the cell samples and the isolated PBS fractions were recorded on a UV-9000S spectrophotometer with a slit width of 1 nm in a 2-mm cuvette with high scattering property. At the corresponding peak wavelengths, molar extinction coefficients of 1185 $mM^{-1}cm^{-1}$ and 770 $mM^{-1}cm^{-1}$ were used for a trimer of PC (620 nm) and APC (650 nm), respectively. According to the absorption spectra of CPC [21], the molar extinction coefficient of 266 $mM^{-1}cm^{-1}$ was used for a trimer of PC (650 nm), while the molar extinction coefficient of 295 $mM^{-1}cm^{-1}$ was used for a trimer of APC in 620 nm according to the absorption spectra of APC [22]. The concentrations of CPC and APC were calculated according to established methods [16,23]. The equations used were:

$$A_{620} = \varepsilon_{CPC}^{620} C_{cpc} + \varepsilon_{APC}^{620} C_{APC}$$
$$A_{650} = \varepsilon_{CPC}^{650} C_{CPC} + \varepsilon_{APC}^{650} C_{APC}$$

3. Fluorescence Measurements

3.1 Fluorescence Emission Spectra

Spectra were acquired using an F-320 Fluorolog spectrofluorimeter, with slit widths set at either 5 or 10 nm. *Synechocystis* WT and mutant strains were cultivated under normal light until reaching an optical density of A730~0.8. For measurement, the chlorophyll a (Chl a) concentration of the cell suspensions was adjusted to either 3 or 5 µg/mL, corresponding to the excitation wavelengths of 580 nm or 430 nm, respectively. Subsequently, 800 µL aliquots of the adjusted cells were dark-adapted for 5 minutes in fresh BG11 medium prior to spectral recording. All experiments were performed with at least three independent biological replicates.

The 77-K fluorescence emission spectra were monitored using a Horiba Fluorolog spectrofluorimeter with a slit width of 8 nm. The cells at CChl = 3 µg/mL (580 nm excitation) were collected by centrifugation and suspended in an equivalent volume of fresh BG11 containing 40% (v/v) glycerol and 25 mM HEPES-NaOH (pH 7.5). In all cases, whole cells were dark-adapted for 15 min before the measurements. Then, the spectra were recorded corresponding to State II. For State I spectra, cells were illuminated with 55 µmol photons $m^{-2}s^{-1}$ of blue light for 5 min. Then, 800 µL suspensions were quickly frozen in quartz tubes by immersion in liquid nitrogen for 10 s. The excitation was measured at 580 nm, and emission was scanned at 600–800 nm [24,25]. Date are from at least three biological replicates.

3.2 A Pulse Amplitude-Modulated Fluorometer (PAM) Fluorometer

The light response curves, NPQ, and state transitions were monitored on a PAM fluorometer (PAM 2500; Walz, Effelrich, Germany) [26,27]. Mutant and WT cells were grown under similar conditions (A730 = 0.6) and estimated on dark-adapted (15 min) whole cells at a chlorophyll concentration of 3 mg/L. F0 is a minimal fluorescence level determined by illuminating dark-adapted cells with a low intensity of red-modulated light (pulses of 1 s, 1.6 kHz, 0.024 µmol photons m^2s^{-1}). For the measurements of state transitions [28], cells were dark-adapted, irradiated with blue (55 µmol photons m^2s^{-1}) or orange light (20 µmol photons m^2s^{-1}), and subjected to saturating pulses (2000 µmol photons m^2s^{-1}, 30 s) to measure the F_m' levels (maximum fluorescence under illumination).

All NPQ induction and recovery experiments were carried out in the presence of chloramphenicol (30 g/mL), a protein synthesis inhibitor, to inhibit protein synthesis [26]. For the measurements of the light response curve, cells (CChl = 20–30 mg/L) were irradiated with various intensities (0–1400 µmol photons m^2s^{-1}) after dark adaptation (15 min) and then subjected to saturating pulses (2000 µmol photons m^2s^{-1}, 30 s) to measure the F_m' levels. The initial slope of the rapid light response curve (alpha), the maximal rate of electron transfer (ETRmax), and the minimal saturated light intensity at semi-saturated light intensity (Ik) were calculated from the PAM data using the analysis software [29,30]. Data are presented as mean ± standard deviation (SD).

3.3 Protein Assay

Protein concentration was quantified using the Bradford method [31] with bovine serum albumin (BSA) as a standard. The proteins from sucrose-containing fractions were precipitated by 50% (NH4)2SO4 and collected by centrifugation to remove the sucrose. Then, the samples were diluted with distilled water and precipitated by 10% trichloroacetic acid (TCA) to remove the ammonia. The remaining TCA was removed by acetone extraction. Subsequently, the obtained samples were dried, solubilized in the sample buffer [32], and analyzed by SDS-PAGE using Laemmli buffer system [33]. Finally, the proteins were stained with Coomassie brilliant blue [34].

3.4 Isolation of PBSs

PBSs were isolated from *Synechocystis* cells by an ultracentrifugation-based protocol [35]. Briefly, cells were lysed with 2% (v/v) Triton X-100, and the lysate was clarified by centrifugation to remove unbroken cells, debris, and chlorophyll. The resulting supernatant (2 mL) was then layered onto sucrose step-gradients for ultracentrifugation. The gradients, prepared in 12-mL tubes with 0.8 M KPB (pH 7.2), consisted of 1 mL of 2.0 M, 2.5 mL of 1.0 M, 2 mL of 0.75 M, 2 mL of 0.5 M, and 1.5 mL of 0.25 M sucrose solutions. Centrifugation was performed at 230,000 ×g for 13 h at 18 ℃ using a P40ST rotor (Hitachi CP80-WX ultracentrifuge). The distinct blue bands containing PBSs were collected and stored at 4 ℃ in sucrose solution for analysis within 48 hours. PBS isolations were performed from at least three independent cultures per mutant.

3.5 The Electron Microscopy (TEM)

Electron microscopy was performed on a HITACHI H-7650 transmission electron microscope operated at 100 kV. The images were recorded with a 1024 × 1024 CCD camera at a magnification of 100,000×. PBS preparations were negatively stained with 2% uranyl acetate by droplet method [7]. Drops of about 5 µL, containing the samples at OD at 620 nm [Δ(*arm2(6-36)/rep3*) was 0.02 OD, Δ(*rep3*) was 0.05 OD] in 0.8 M potassium phosphate (pH 7.2) were deposited on the surface of glow-discharge and carbon-coated copper grids. After 1–3 min, the droplets were stained with 2% uranyl acetate.

4. Results

4.1 The Helix-Loop-Helix Element of Arm2 in Synechocystis Mediates the Longitudinal Assembly of PBSs

Arm2 in apo-protein of L_{CM} (ApcE) from *Synechocystis* constitutes 401–534 aa. Thus, we re-numbered Arm2 as 1–134 aa (Fig. 1A). Strikingly, the amino acid sequence of Arm2 of the red alga *Griffithsia pacifica* was highly similar to that of *Synechocystis* (**Supplementary Fig. 1A**). Based on the 3.5 Å PBS structure from the red alga *Griffithsia pacifica* [8], the conservative motif of Arm2(6–36) in *Griffithsia pacifica* formed the super-secondary structure of α-helix/loop/α-helix (**Supplementary Fig. 1B**) and the rest of the molecule forms random coils. Arm2 in *Synechocystis* also forms this super-secondary structure, i.e., a loop (Arm2(18–28)) linking two α-helices (Arm2(6–17) and Arm2(29–36)), followed by random coils **Supplementary Fig. 1C**). To investigate the functions of Arm2, we generated a series of *Synechocystis* mutants-Δ(*rep3*), Δ(*arm2/rep3*), Δ(*rep2/rep3*), and Δ(*arm2/rep2/rep3*)-by selectively deleting the Rep3, Arm2/Rep3, Rep2/Rep3, and Arm2/Rep2/Rep3 domains, respectively, from the ApcE protein (Fig. 1). In order to locate the functional motifs in Arm2, a set of mutants with partial truncations within Arm2 were constructed by truncating an amino acid fragment of Arm2 based on Δ(*rep3*) mutant (Fig. 1). Complete segregation of all mutants was confirmed by PCR analysis (**Supplementary Fig. 2**). The traces of the 1.5- to 2.5-kbp fragments were detected in WT but not the mutants, indicating complete segregation.

The assembly of PBSs in the absences of Rep3 remains a subject of debate. The classic model of PBSs of *Synechocystis* suggests that Pep3 is essential for Cylinder 3 attachment, with its lost resulting in a simple, two-cylinder core (Cylinder1 and 2) [7]. In contrast, the structural study on PBS on the red alga *Griffithsia pacifica* [8], Cylinder3 is lost in the absence of Rep3, and then Cylinder1 and 2 are disconnected. Given the symmetry of PBSs, Cylinder1 and 2 are same, and we would only isolate a simple PBS of Cylinder1 or 2 in the core. Next, we isolated the PBSs from Δ(*rep3*): the ultracentrifugation of PBSs retrieved three fractions in a molar ratio of 1.47:1:7.17 (Fig. 2A and **Supplementary Table 2**). The major fraction showed maximal absorption at 620 nm and maximal fluorescence at 668 nm at room temperature and at 684 nm at 77 K. Similarly, the two minor fractions absorbed maximally at 654 nm and exhibited fluorescence at 664–668 nm at room temperature and at 680–684 nm at 77 K. The data indicated the following: (1) while dismantled CPC was barely detected, a small part of the dismantled PBS cores could be isolated. In the isolated cores, the energy absorbed by APC could be efficiently transferred to the two terminal emitters, such that the cores were not damaged. (2) In the isolated PBSs, the energy absorbed by CPC could efficiently be transferred to the two terminal emitters, such that the PBSs remained intact. The SDS-PAGE (**Supplementary Fig. 3A lane 3**) showed that the major fraction PBSs of Δ(*rep3*) assembled intact similar to WT (**Supplementary Fig. 3I lane 1**), except for a truncated ApcE. The photosynthetic capacity parameters (**Supplementary Fig. 4**, **Supplementary Tables 3,4**) and cell fluorescence spectra at room temperature (**Supplementary Fig. 5A,D** and **Supplementary Table 5**) and 77 K (**Supplementary Fig. 6A,D** and **Supplementary Table 5**) of Δ(*rep3*) were similar to those of WT, further supporting the intactness and functionality of the PBSs. However, the absorption spectra of Δ(*rep3*) showed that this mutant had 1.3 times less phycobiliprotein per chlorophyll than WT (**Supplementary Fig. 7A** and **Supplementary Table 5**), indicating that the deletion of Rep3 of ApcE might affect the assembly of PBSs or phycobiliprotein biosynthesis [19]. Considering the smaller size observed by TEM (**Supplementary Fig. 8**) and the structural model from Liu *et al*. [12], we interpret these results as being most consistent with the isolation of a simple, one-cylinder PBS.

We next analyzed PBSs from the double mutant Δ(*arm2(6–36)/rep3*). Ultracentrifugation on a sucrose gradient (Fig. 2A) indicated that the PBSs of Δ(*arm2(6–36)/rep3*) showed a major fraction at 0.25 M and a minor fraction suspended at 0.5–0.75 M sucrose gradient; the two fractions were in 5.59:1 molar ratio (**Supplementary Table 2**). The major fraction had an absorbance of 620 nm and a fluorescence maxima at 658 nm at room temperature, while the 77 K fluorescence peak shifted to 666 nm (Fig. 2B–D). The minor fraction had the typical absorption and fluorescence maxima of CPC at 620 nm and 642 nm, respectively, and the 77 K fluorescence shifted to 654 nm (Fig. 2E–G). Importantly, the PBSs of Δ(*arm2(6–17)/rep3*) and Δ(*arm2(29–36)/rep3*) presented characteristics at the same sucrose gradient similar to those of Δ(*arm2(6–36)/rep3*) (Fig. 2). These results indicated that (1) a specific amount of the CPC rods was dismantled from the PBS cores in these mutants. These findings could question the integrity of PBSs in these mutants; (2) the major fraction contained a simple, partially dismantled PBS consisting of only CPC and APC in 1.66 $\pm$ 0.29 molar ratio, but the energy absorbed by CPC in this simple PBS was transferred to APC. Hence, it could be speculated that in the simple PBSs, one APC hexamer binds three CPC trimers, or two APC hexamers (disks) bind three CPC hexamers (disks); (3) for the three mutants, the truncation of the helix-loop-helix of 6–36 aa, the helix of 6–17, or the helix of 29–36 from Arm2 presented a similar phenotype of PBS, i.e., the helix-loop-helix, or one of the helix exerted a similar role in PBS assembly, consistent with our previous report [11].

According to the PBS structure from the red alga *Griffithsia pacifica* [8], the Arm2 element of helix-loop-helix is inserted between one normal APC disk and two APC disks, one of which has a L_{CM} terminal emitter and the other has

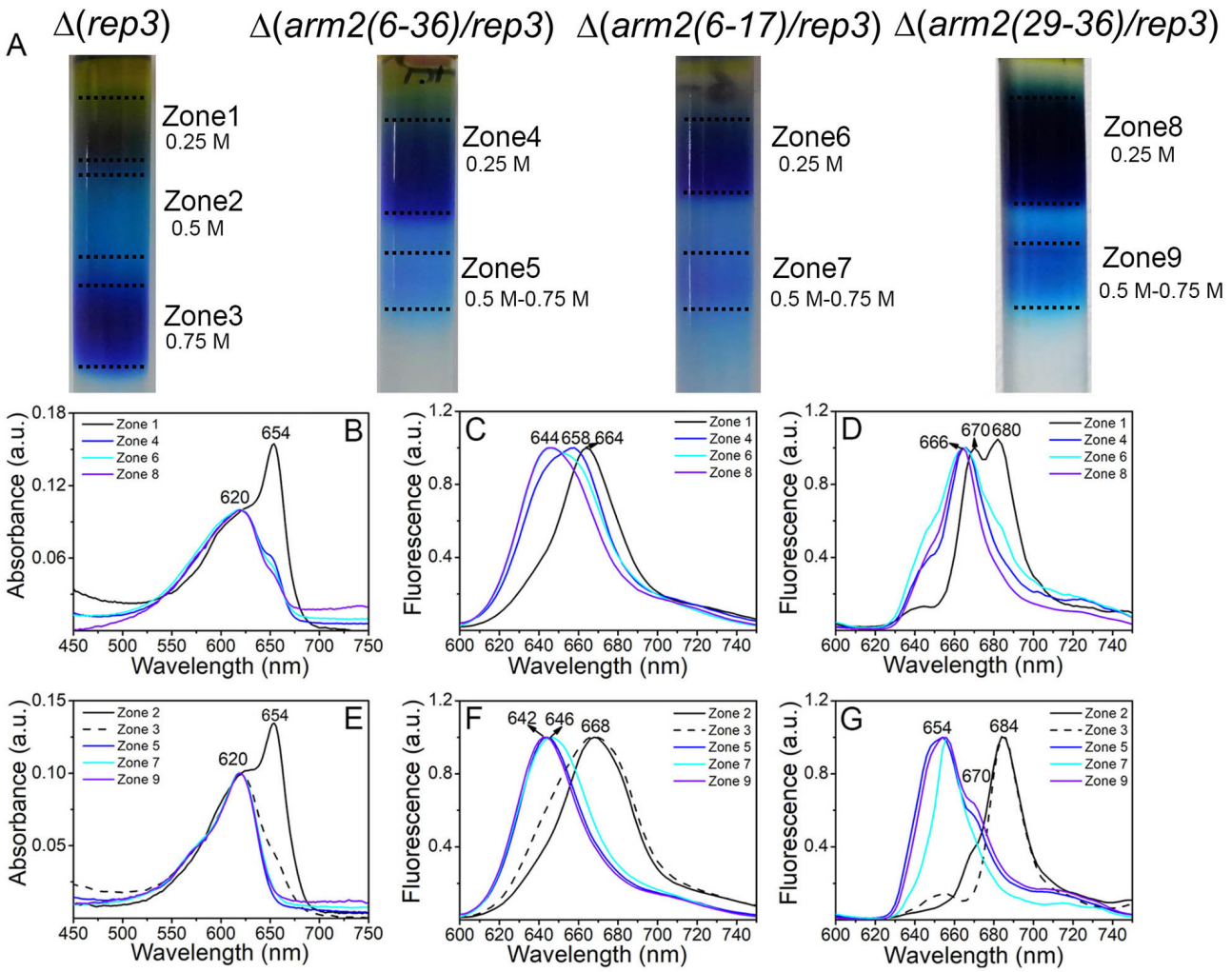

Fig. 2. Characterization of the PBSs of Δ(*rep3*), Δ(*arm2(6–36)/rep3*), Δ(*arm2(6–17)/rep3*), and Δ(*arm2(29–36)/rep3*) mutants from *Synechocystis* PCC 6803. Sucrose gradient ultracentrifugation (A), absorption (B,E) and fluorescence emission spectra at room temperature (C,F) and 77 K (D,G) of the PBSs of the four mutants. The samples (B–D) of Δ(*rep3*) (Zone1, black), Δ(*arm2(6–36)/rep3*) (Zone4, blue), Δ(*arm2(6–17)/rep3*) (Zone6, cyan), and Δ(*arm2(29–36)/rep3*) (Zone8, violet) were obtained from 0.25 M sucrose gradient. The samples (E–G) of Δ(*rep3*) (Zone2 and Zone3, solid and dash black), Δ(*arm2(6–36)/rep3*) (Zone5, blue), Δ(*arm2(6–17)/rep3*) (Zone7, cyan), and Δ(*arm2(29–36)/rep3*) (Zone9, violet) were obtained from 0.5–0.75 M or 0.75 M sucrose gradient. The absorption spectra were normalized at 620 nm, while the fluorescence emission spectra were normalized at their main peak position. All the fluorescence emission spectra were measured by excitation at 580 nm. The sucrose gradient ultracentrifugation of the Δ(*arm2(18–29)/rep3*) mutant was not carried out due to its liability to reverse mutation.

AP-B terminal emitter in one basal cylinder (i.e., Cylinder1 or 2). When one helix or both helices of Arm2 were truncated, a simple PBS containing only APC/CPC was generated such that the other longitudinal half PBS with the APC disks harboring the terminal emitters (L_{CM} and ApcD) was lost. The cell spectra showed a high fluorescence of these mutants at 660 nm (**Supplementary Fig. 5A–C**) that disappeared completely at 683 nm (**Supplementary Fig. 5D–F**). Upon excitation at 430 nm and at 580 nm, the corresponding fluorescence confirmed that the energy transfer from APC to the terminal emitters of PBSs was disrupted [19]. Moreover, due to the absence of terminal emitters, the energy transfer from the PBSs to PSs was disrupted (**Supplementary Fig. 5**). The photosynthetic capacities (**Supplementary Table 3**) were much lower than those of Δ(*rep3*) and WT. Consequently, the mutants Δ(*arm2/rep3*), Δ(*arm2(6–36)/rep3*), Δ(*arm2(6–17)/rep3*), and Δ(*arm2(29–36)/rep3*) of the damaged Arm2 element grew poorly under photoautotrophic conditions but are capable of growing photomixotrophically in the culture media supplemented with 10 mM glucose (**Supplementary Fig. 4**). **Supplementary Table 4** shows that when the chlorophyll content is maintained, the level of F_0 in these mutants is 2- to 5-fold higher than that of Δ(*rep3*), which

is consistent with the high fluorescence intensity of these mutants (**Supplementary Fig. 5**). Reportedly, a specific number of uncoupled PBSs may be one of the reasons for increased F_0 in cyanobacteria [19,36,37]. The results suggested Arm2 as a putative candidate for PBSs binding thylakoid membranes [13]. Also, the generation of small PBSs containing only APC/CPC effectuated a weak association between PBSs and thylakoid membranes.

Therefore, the Arm2 element is responsible for the longitudinal assembly of PBSs. The loss of the element results in the dissociation of half of the PBS harboring the terminal emitters, while the other half, i.e., the simple PBS with only APC and CPC is retained in the cells. The cell spectra showed the absence of 77 K fluorescence at 684–685 nm corresponding to the terminal emitters (**Supplementary Fig. 6**, **Supplementary Table 5**). Hence, the dissociated parts of the PBSs could be degraded via specific phycobiliprotein degradation routes [38,39]. One terminal emitter, ApcD, could undergo de-chromophorylation for its degradation [22]. The other terminal emitter, L_{CM}, degraded slowly, and hence, a little L_{CM} (the small peak at ~670 nm in Fig. 2 and **Supplementary Fig. 6**) was detected in the isolated PBSs from some mutants of the damaged Arm2 element.

To further investigate the roles of the motif of Arm2(6–36), we isolated the PBSs of Δ(*arm2/rep3*), Δ(*rep2/rep3*), and Δ(*arm2/rep2/rep3*). Their ultracentrifugation (**Supplementary Fig. 9**) showed a similar fraction pattern compared to Δ(*arm2(6–36)/rep3*), and the spectra of the fractions were also similar to those of Δ(*arm2(6–36)/rep3*). The coincidence between Δ(*arm2/rep3*) and Δ(*arm2(6–36)/rep3*) confirmed Arm2(6–36) as the key element of Arm2. According to the PBS structure of the red alga *Griffithsia pacifica* [8] and a PBS core conformation similar to that suggested by Liu *et al*. [12], the truncation of Rep2 and 3 dismantles the APC disk of Cylinder3 and basal cylinders and retains the APC disk with L_{CM} of basal cylinders. Although the spectra showed 77 K fluorescence at ~680 nm (**Supplementary Fig. 9D**), which would be L_{CM} in a trimer [40], the fluorescence degree was too small compared to that at 666 nm of APC. Thus, the energy absorbed by APC could only slightly be transferred to L_{CM}, indicating that (1) the simple PBSs having only APC and CPC were predominant and/or (2) the APC disks with and without L_{CM} were not well connected.

4.2 Arm2(37–67) Facilitates CPC Rod Attachment at the Cores and Arm2(68–129) has no Remarkable Effects on the Assembly of PBSs

The ultracentrifugation of Δ(*arm2(37–67)/rep3*) generated a fraction pattern similar to that of Δ(*arm2(6–36)/rep3*). On the other hand, the minor fraction at 0.25 M sucrose gradient showed similar absorption and fluorescence at 680 nm fluorescence (**Supplementary Fig. 10**), the fraction suspended at the 0.5–0.75 M sucrose gradient showed maximal absorption at 620 nm, fluorescence at 650 nm at room temperature and at 656 nm at 77 K, which corresponded to CPC, as verified by SDS-PAGE (**Supplementary Fig. 3J**). The molar ratio of minor:major fraction was 1:1.57 (**Supplementary Table 6**), indicating that CPC rods mainly dissociated from the cores in Δ(*arm2(37–67)/rep3*) and that the 36–67-aa motif, although in random coils, might be responsible for the attachment of CPC rods at the cores (**Supplementary Fig. 1**).

Conversely, Δ(*arm2(68–98)/rep3*) and Δ(*arm2(99–129)/rep3*) showed an ultracentrifugation pattern different from the mutants of the damaged Arm2 but similar to that of Δ(*rep3*). Among the three fractions, the two minor fractions at 0.25 and 0.5 M sucrose gradient absorbed maximally at 654 nm and 620 nm with an obvious 654 nm peak that exhibited fluorescence at 661–672 nm at room temperature and at 683–684 nm at 77 K, respectively (**Supplementary Fig. 10B–G**). In addition, the major fraction at 0.75 M sucrose gradient had similar characteristic absorption and fluorescence at room temperature and 77 K fluorescence spectra as the PBSs from intact Δ(*rep3*) and WT (**Supplementary Fig. 10H–J**). Therefore, the energy absorbed by CPC could be transferred efficiently to the terminal emitters. The cell spectra also showed an efficient energy transfer *in vivo* from CPC to AP-B (**Supplementary Fig. 6**, **Supplementary Table 5**). Furthermore, due to the truncation, the fluorescence at 684–685 nm assigned to the terminal emitter, AP-B, decreased gradually according to the order of Δ(*rep3*), Δ(*arm2(99–129)/rep3*), and Δ(*arm2(68–98)/rep3*) (**Supplementary Fig. 10J**).

4.3 The Arms Helix-Loop-Helix Element is Essential for State Transitions and OCP-Associated NPQ

Cyanobacterial NPQ and state transitions affect the balance between energy transfer and dissipation within the PBSs and the distribution of excitation energy from the PBSs to the PSs [41]. Experimentally, states I and II are induced by blue LL and orange LL irradiation, respectively, such that the energy is preferentially transferred to photosystem I (PSI) and from PBS to PSII [42]. When state transitions occur at a low irradiation intensity, the high irradiation intensity quenches the non-photochemical PBSs, triggered by OCP [19,43].

Pulse amplitude-modulated fluorometer (PAM) fluorescence technique is often used to study the energy transfer between PBSs and PSs. In PAM measurements, dark-adapted cells have a low dark maximal fluorescence (F_{md}), but when they are continuously irradiated by blue LL (55 μmol photons m^2/s), the F_m' increases rapidly and arrives at a maximal F_m' fluorescence level (F_{mb}'), indicating that the cells have undergone the transition to state I. Thus, the ratio of F_{vb}/F_{vd} ($F_V = F_m - F_0$) indicated the ability of mutants to transform state II→state I. When the Blue LL light-adapted cells are irradiated with orange light (20 μmol photons m^2s^{-1}), the decrease in F_m' indicates the ability

of mutants to transform from state I→state II [24,44,45]. Herein, we compared the state transition performance of WT and mutants: the ratio of F_{vb}/F_{vd} was consistent (approximately 15), and the F_m' decreased rapidly in WT and Δ(*rep3*) mutant (**Supplementary Fig. 11**). However, the ratio of F_{vb}/F_{vd} in Δ(*arm2/rep3*) and Δ(*arm2(6–36)/rep3*) mutants was negative (Fig. 3C,D), and that in the mutants without the Arm2(6–17) or Arm2(29–36) motif was lower than that in Δ(*rep3*) and WT (Fig. 3E,F), implying a strongly-weakened ability of these mutants to perform state II→state I. This phenomenon was supported by the results that the 77 K fluorescence emission spectra of blue-adapted WT and Δ(*rep3*) cells had a high PSII fluorescence band with respect to dark-adapted cells, while the PSII fluorescence peak of Δ(*arm2/rep3*) and Δ(*arm2(6–36)/rep3*) mutants or Δ(*arm2(6–17)/rep3*) and Δ(*arm2(29–36)/rep3*) mutants showed only a slight increase (Fig. 4) [19,36,46]. On the contrary, the ratio of F_{vb}/F_{vd} in the other mutants of the damaged Arm2 was higher than that in Δ(*rep3*) (**Supplementary Fig. 11D–F**). Interestingly, under orange LL, the F_m' of all mutants of the damaged Arm2 did not decrease, indicating that the transition from transition I to state II cannot occur (Fig. 3 and **Supplementary Fig. 11**). Based on these results, we concluded that (1) damaging the helix-loop-helix element of Arm2 produced simple APC/CPC PBSs, effectuating a weak association between PBSs and the thylakoid membrane. This prevents the state I transition from state II and the energy transfer between the two PSs; (2) damaged Arm2 disrupted the connection between APC disk and APC disk with terminal emitters, such that the energy transfer from the PBSs to PSs was perturbed and the transition from state I to state II was impaired. The terminal emitters are responsible for transferring the absorbed energy to the reaction centres and plays a crucial part in energy migration and affects state transitions [47].

Next, the NPQ performance of WT and mutants was compared (Fig. 5). The results showed strong blue light-induced PBS fluorescence quenching (about 14%) in WT, while that in Δ(*arm2/rep3*) or Δ(*rep3*) mutants was low (about 0.69% or 4.96%) (Fig. 5G). Interestingly, the mutants of the damaged helix-loop-helix element of Arm2 showed an NPQ performance similar to the WT (Fig. 5A–F), while the remaining mutants showed a phenotype similar to Δ(*rep3*) mutants (**Supplementary Fig. 12C–E**). When dark-adapted cells were exposed to white high light (HL) directly, Fluorescence quenching was reversible in all strains in the darkness (Fig. 5H and **Supplementary Fig. 12F**). Importantly, WT and Δ(*arm2/rep3*) recovered from NPQ a similar rate but 3-fold faster than Δ(*rep3*), while Δ(*arm2(6–36)/rep3*), Δ(*arm2(6–17)/rep3*), and Δ(*arm2(29–36)/rep3*) recovered faster than Δ(*rep3*). These results support the following findings: (1) the damaged helix-loop-helix element of Arm2 produced small APC/CPC PBSs, which had the more packed conformation increased the probability of energy transfer between different rods [47] and might allow OCP to approach the PBSs closely in some directions, such that OCP-dependent NPQ is significant; (2) the integrity of PBSs is crucial for strong binding of activated OCP. The activated OCP may be loosely bound by the small PBSs and easily released from them compared to WT PBSs.

5. Discussion

Our study establishes the critical role of the Arm2 helix-loop-helix element in the longitudinal assembly and functional integrity of the PBS in *Synechocystis* sp. PCC 6803. The structural and functional defects observed in our Arm2 truncation mutants provide new insights into PBS architecture, state transitions, and photoprotection.

Structural Role of Arm2 and PBS Assembly. Our data demonstrate that the helix-loop-helix element of Arm2 (residues 6–36) is essential for connecting the two longitudinal halves of the PBS core. Truncation of this element leads to the specific loss of the half-core containing the terminal emitters L_{CM} and ApcD, resulting in simplified APC/CPC complexes (Fig. 2, **Supplementary Figs. 5,6**). This phenotype aligns with the proposed location of Arm2 in the Griffithsia pacifica PBS structure [8], where it bridges APC hexamers within a basal cylinder. Our previous study, informed by homology modeling [12] and based on low-resolution molecular structure of cyanobacterial PBS [48], positions the *Synechocystis* Arm2 helix-loop-helix similarly, providing a structural basis for its essential role in core integrity. The CPC/APC molar ratio of ~1.66 in these simplified PBSs (**Supplementary Table 2**) is consistent with a structure where one APC hexamer associates with three CPC hexamers, a configuration potentially favored in the absence of the full core constraint. The subsequent degradation of the dissociated emitter-half suggests active quality control mechanisms for unassembled PBS components [38,39]. Beyond the core, the Arm2(37–67) region, though unstructured, appears to facilitate the attachment of CPC rods to the core (**Supplementary Fig. 10**), highlighting the multi-functional nature of this linker domain. In contrast, the distal regions of Arm2(68–129) have minimal impact on assembly under our conditions.

Implications for State Transitions. A key finding is the abolition of state transitions in mutants lacking the Arm2 helix-loop-helix element (Figs. 3,4). The current understanding of state transitions involves redistribution of excitation energy between PSII and PSI, potentially through PBS movement [42,49]. While some models propose lateral PBS displacement or detachment from the membrane [49,50], our results suggest that longitudinal rearrangements within the PBS core itself, facilitated by Arm2, are crucial. The loss of state transitions in our mutants likely stems from a dual defect: (1) the physical absence of one terminal emitter-bearing half-core, which disrupts the energy delivery network to both photosystems, and (2) the

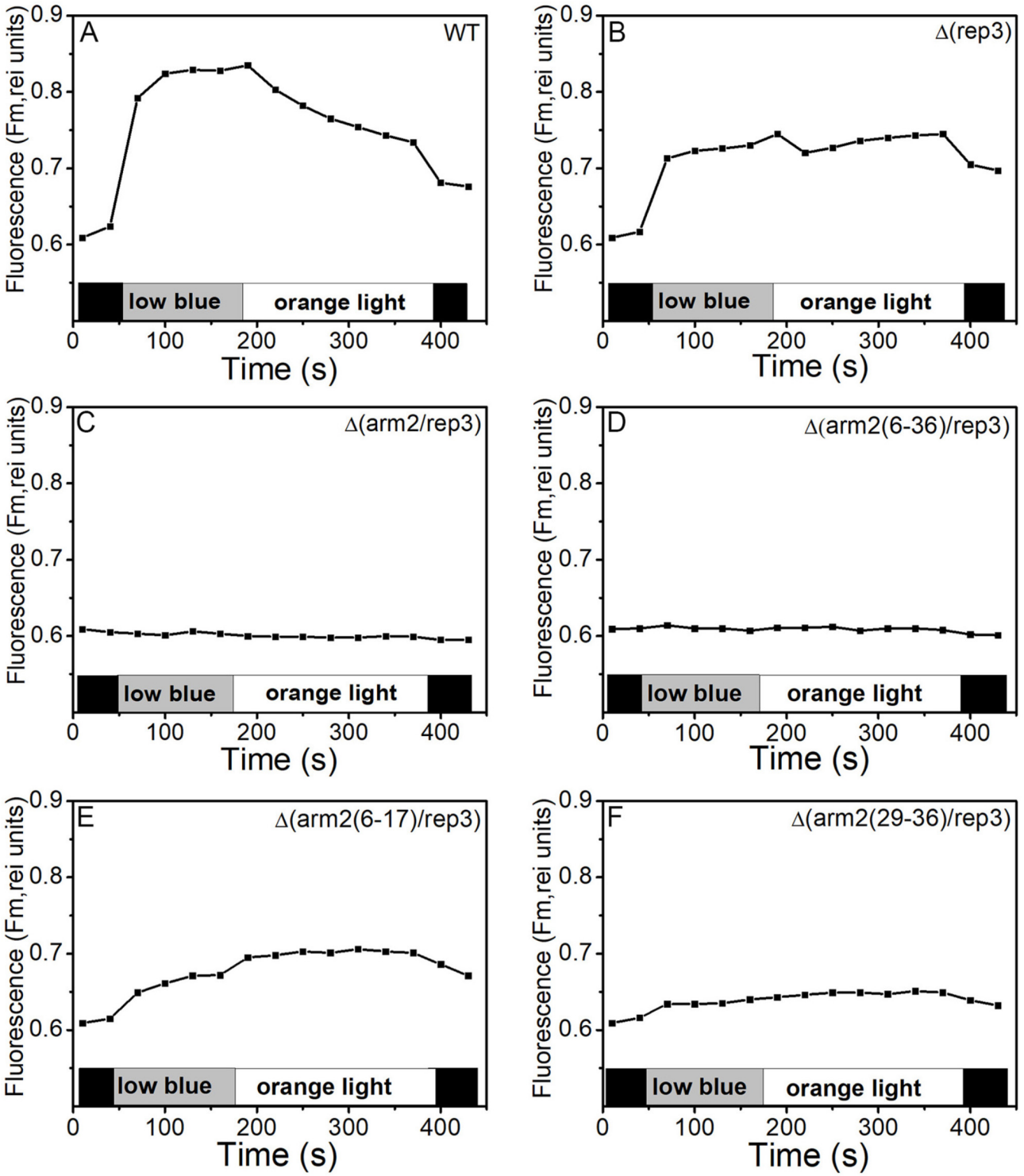

Fig. 3. State transitions in WT, Δ(*rep3*), Δ(*arm2/rep3*), Δ(*arm2(6–36)/rep3*), Δ(*arm2(6–17)/rep3*), and Δ(*arm2(29–36)/rep3*) mutants from *Synechocystis* PCC 6803. The fluorescence changes were followed with a PAM fluorometer. Dark-adapted cells containing 3 µg/mL Chl in BG11 were stimulated with blue LL (55 µmol photons $m^{-2}s^{-1}$) and orange (609 nm) LL (20 µmol photons $m^{-2}s^{-1}$). Typical experiments are shown for *Synechocystis* WT (A), Δ(*rep3*) (B), Δ(*arm2/rep3*) (C), Δ(*arm2(6–36)/rep3*) (D), Δ(*arm2(6–17)/rep3*) (E), and Δ(*arm2(29–36)/rep3*) (F) mutant cells. The saturating pulses were separated by 30 s with 2000 µmol photons $m^{-2}s^{-1}$. Traces are from one representative experiment and are consistent with the results from two other independent biological replicates (n = 3).

weakened association of the simplified PBSs with the thylakoid membrane, potentially impeding the physical mobility or conformational changes required for state transitions. Our data do not rule out detachment/reattachment mecha-

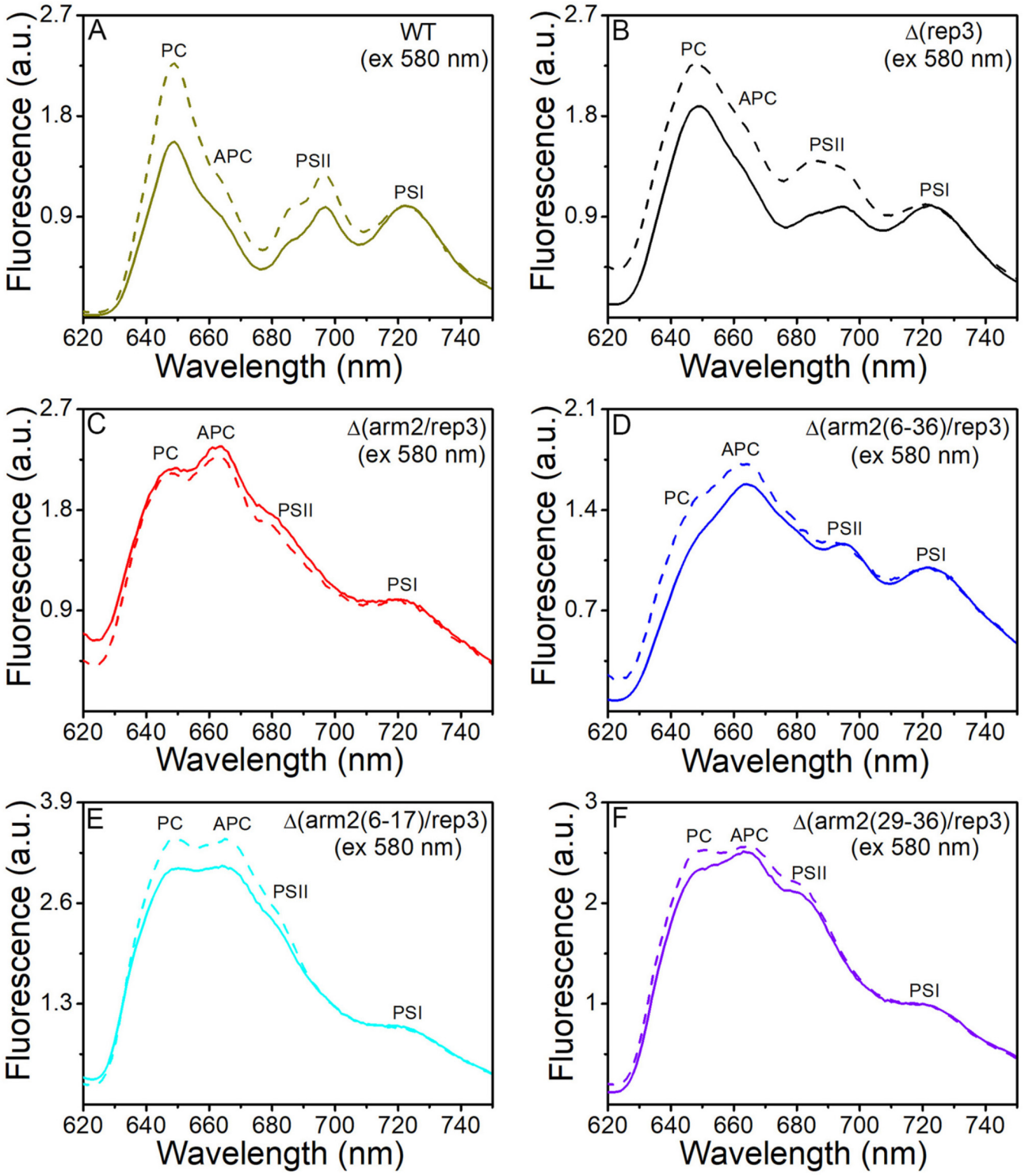

Fig. 4. State transitions in WT, Δ(*rep3*), Δ(*arm2/rep3*), Δ(*arm2(6–36)/rep3*), Δ(*arm2(6–17)/rep3*), and Δ(*arm2(29–36)/rep3*) mutants from *Synechocystis* PCC 6803. 77 K fluorescence emission spectra of dark (solid, State II) and blue-light (dash, state I, 55 µmol photons $m^{-2}s^{-1}$) adapted WT (dark yellow, A), Δ(*rep3*) (black, B), Δ(*arm2/rep3*) (red, C), Δ(*arm2(6–36)/rep3*) (blue, D), Δ(*arm2(6–17)/rep3*) (cyan, E), and Δ(*arm2(29–36)/rep3*) (violet, F) cells. Normalization was carried out at 720 nm. The measurements were recorded at a chlorophyll concentration of 3 µg/mL. All fluorescence emission spectra were measured by excitation at 580 nm. Spectra are from one representative experiment and are consistent with the results from two other independent biological replicates (n = 3). APC, allophycocyanin; PSII, photosystem II; PSI, photosystem I; PC, phycocyanin.

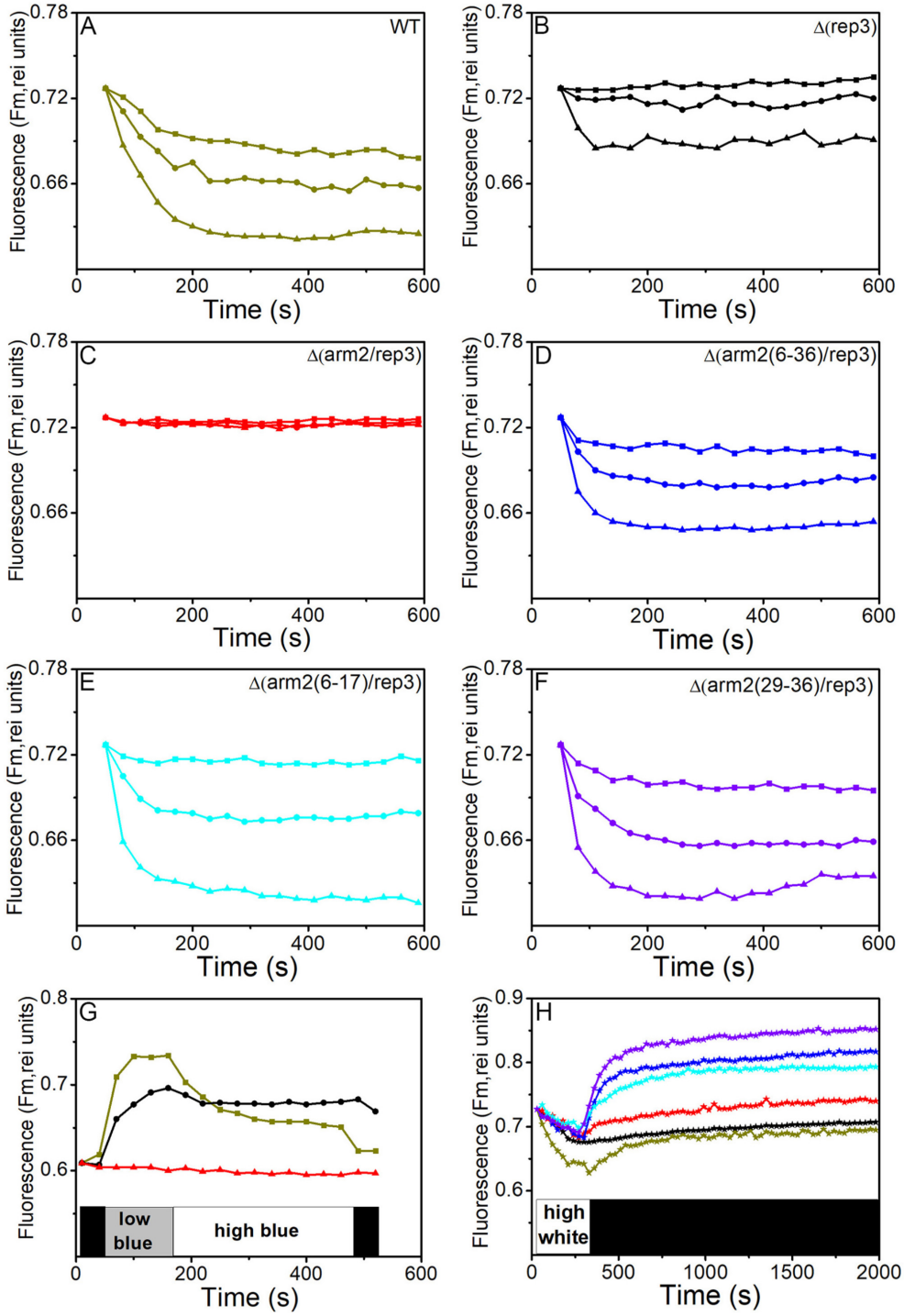

Fig. 5. Changes in fluorescence levels induced by different intensities of blue light and dark recovery of quenched fluorescence measured in a PAM fluorometer. Dark-adapted *Synechocystis* WT cells (dark yellow, A), Δ(*rep3*) (black, B), Δ(*arm2/rep3*) (red, C), Δ(*arm2(6–36)/rep3*) (blue, D), Δ(*arm2(6–17)/rep3*) (cyan, E) and Δ(*arm2(29–36)/rep3*) (violet, F) mutant cells were illuminated with strong blue light intensities (460 nm) at 127 (squares), 307 (circle), and 503 (triangle) µmol photons $m^{-2}s^{-1}$ to induce the quenched state. (G) Dark-adapted *Synechocystis* WT cells (dark yellow), Δ(*rep3*) mutant cells (black), and Δ(*arm2/rep3*) mutant cells (red) were illuminated successively with a low-intensity blue light (460 nm, 55 µmol photons $m^{-2}s^{-1}$) and a high-intensity blue light (460 nm, 503 µmol photons $m^{-2}s^{-1}$). (H) Dark-adapted cells of six mutants shown above containing 3 µg/mL Chl were illuminated directly with white HL (20 µmol photons $m^{-2}s^{-1}$) for 5 min and then kept in the darkness. Saturating pulses were separated by 30-s intervals with 2000 µmol photons $m^{-2}s^{-1}$. All the experiments were carried out in the presence of chloramphenicol. Traces are from one representative experiment and are consistent with the results from two other independent biological replicates (n = 3).

nisms [49,50] but emphasize that the integrity of the core structure, maintained by Arm2, is a prerequisite for these processes.

OCP-mediated NPQ and PBS Integrity. The mutants with damaged Arm2 exhibited faster recovery from OCP-related NPQ (Fig. 5H), despite retaining significant quenching capacity. This accelerated recovery is consistent with a model where the simplified PBSs, due to their altered conformation and/or reduced size, bind the activated OCP with lower affinity, allowing for its more rapid release upon signal cessation. The core region, particularly the APC cylinders, is a proposed binding site for OCP [51–53]. Structural alterations in this region, as caused by Arm2 truncation, could directly affect OCP docking stability. While this interpretation is plausible, direct evidence from OCP binding affinity assays with purified WT and mutant PBSs would be needed to conclusively support this hypothesis, representing an important direction for future research.

In summary, the Arm2 linker in L_{CM} acts as a critical structural organizer for the PBS core. Its helix-loop-helix element is indispensable for longitudinal assembly, state transitions, and fine-tuning OCP-related photoprotection, underscoring the importance of linker domains in the structure and function of massive photosynthetic antenna complexes.

6. Conclusion

This study demonstrates that the helix-loop-helix element of Arm2 is critical for the longitudinal assembly of PBS. Deletion of the Rep3 domain resulted in an intact PBS core comprising only Cylinder1 or 2. Additionally, when one or both helices of Arm2 are truncated, simple PBS containing only APC/CPC could be generated, while the other longitudinal half of PBSs containing the terminal emitters (L_{CM} and ApcD) may be degraded and lost. Consequently, in the isolated Δ(*rep3*) PBSs, the energy absorbed by CPC can be transferred efficiently to the two terminal emitters, rendering the PBSs fully functional. In the mutants of the damaged helix-loop-helix element of Arm2, the energy transfer from APCs to terminal emitters to PSI and II decreases, and photosynthesis is impaired due to the generated simple PBSs APC/CPC, although the energy transfer from CPC to APC is efficient. The simple APC/CPC PBSs ascribed a weak connection between PBSs and thylakoid membrane, which impairs the energy transfer between two PSs, preventing state I transition. Conversely, when Arm2 is damaged, the APC disk and the APC disk harboring the terminal emitters are not well connected, due to which the energy transfer from the PBSs to PSs is perturbed, impairing the transition to state II. Subsequently, the activated OCP binds weakly to PBSs due to the simple APC/CPC PBSs, and post-relaxation, OCP is easily released from simple PBSs. Therefore, the mutants of the damaged helix-loop-helix of Arm2 can still perform OCP-induced-NPQ but recover quickly. In addition to the helix-loop-helix of Arm2, the motif of Arm2(37–67) mediates the association of CPC rods to the PBS core, while the other motifs, Arm2(68–98) and Arm2(99–129) have no remarkable effect on PBS assembly.

Abbreviations

AP-B, allophycocyanin B; APC, allophycocyanin; ApcE, apo-protein of L_{CM}; Chl, chlorophyll; CPC, cyanobacterial phycocyanin; F_0, minimal fluorescence level; F_m, maximal fluorescence level in dark-adapted samples; F_m', maximum fluorescence under illumination; Fs, steady-state fluorescence level; F_{md}, maximum fluorescence in darkness; F_{mb}', maximum fluorescence under blue-light illumination; F_V, variable fluorescence = F_m – F_0; F_{vd}, variable fluorescence in darkness; F_{vb}, variable fluorescence under blue-light illumination; HL, high light; KPB, potassium phosphate buffer; L_{CM}, phycobilisome core-membrane linker; LL, low light; NPQ, non-photochemical quenching; OCP, orange carotenoid protein; PAM, a pulse amplitude-modulated fluorometer; PBS, phycobilisome; PCB, phycocyanobilin; PSI and PSII, photosystem I and II; SDS-PAGE, sodium dodecyl sulfate polyacrylamide gel electrophoresis.

Availability of Data and Materials

The data supporting the results are included in this article and the supporting information files.

Author Contributions

NNN, NC, HHF and XLD contributed to the study conception and design. NNN and NC carried out the studies, participated in collecting data, and drafted the manuscript. HHF and XLD performed the statistical analysis and participated in its design. NNN participated in acquisition, analysis, or interpretation of data and draft the manuscript. All authors read and approved the final manuscript. All authors contributed to editorial changes in the manuscript. All authors have participated sufficiently in the work and agreed to be accountable for all aspects of the work.

Ethics Approval and Consent to Participate

Not applicable.

Acknowledgment

Not applicable.

Funding

This work was supported by the Key Research Projects of Higher Education Institutions in Henan Province (26B230010) and the Research Project of Luoyang Polytechnic (2024046).

Conflict of Interest

The authors declare no conflict of interest.

Supplementary Material

Supplementary material associated with this article can be found, in the online version, at https://doi.org/10.31083/FBL47370.

References

[1] Glazer AN. Adaptive Variations in Phycobilisome Structure. Advances in Molecular and Cell Biology. 1994; 10: 119–149. https://doi.org/https://doi.org/10.1016/S1569-2558(08)60396-3.

[2] Glazer AN. Phycobilisome a macromolecular complex optimized for light energy transfer. Biochimica et Biophysica Acta (BBA)-Reviews on Bioenergetics. 1984; 768: 29–51. https://doi.org/10.1016/0304-4173(84)90006-5.

[3] Gantt E, Grabowski B, Cunningham FX. Antenna Systems of Red Algae: Phycobilisomes with Photosystem ll and Chlorophyll Complexes with Photosystem I. In Light-Harvesting Antennas in Photosynthesis (pp. 307–322). Springer: Dordrecht. 2003. https://doi.org/10.1007/978-94-017-2087-8_10.

[4] Tang K, Ding WL, Höppner A, Zhao C, Zhang L, Hontani Y, *et al*. The terminal phycobilisome emitter, LCM: A light-harvesting pigment with a phytochrome chromophore. Proceedings of the National Academy of Sciences of the United States of America. 2015; 112: 15880–15885. https://doi.org/10.1073/pnas.1519177113.

[5] Peng PP, Dong LL, Sun YF, Zeng XL, Ding WL, Scheer H, *et al*. The structure of allophycocyanin B from *Synechocystis* PCC 6803 reveals the structural basis for the extreme redshift of the terminal emitter in phycobilisomes. Acta Crystallographica. Section D, Biological Crystallography. 2014; 70: 2558–2569. https://doi.org/10.1107/S1399004714015776.

[6] Houmard J, Capuano V, Colombano MV, Coursin T, Tandeau de Marsac N. Molecular characterization of the terminal energy acceptor of cyanobacterial phycobilisomes. Proceedings of the National Academy of Sciences of the United States of America. 1990; 87: 2152–2156. https://doi.org/10.1073/pnas.87.6.2152.

[7] Arteni AA, Ajlani G, Boekema EJ. Structural organisation of phycobilisomes from *Synechocystis* sp. strain PCC6803 and their interaction with the membrane. Biochimica et Biophysica Acta. 2009; 1787: 272–279. https://doi.org/10.1016/j.bbabio.2009.01.009.

[8] Zhang J, Ma J, Liu D, Qin S, Sun S, Zhao J, *et al*. Structure of phycobilisome from the red alga Griffithsia pacifica. Nature. 2017; 551: 57–63. https://doi.org/10.1038/nature24278.

[9] Ducret A, Müller SA, Goldie KN, Hefti A, Sidler WA, Zuber H, *et al*. Reconstitution, characterisation and mass analysis of the pentacylindrical allophycocyanin core complex from the cyanobacterium Anabaena sp. PCC 7120. Journal of Molecular Biology. 1998; 278: 369–388. https://doi.org/10.1006/jmbi.1998.1678.

[10] Capuano V, Thomas JC, Tandeau de Marsac N, Houmard J. An in vivo approach to define the role of the LCM, the key polypeptide of cyanobacterial phycobilisomes. The Journal of Biological Chemistry. 1993; 268: 8277–8283.

[11] Niu NN, Lu L, Peng PP, Fu ZJ, Miao D, Zhou M, *et al*. The phycobilisome core-membrane linkers from *Synechocystis* sp. PCC 6803 and red-algae assemble in the same topology. The Plant Journal: for Cell and Molecular Biology. 2021; 107: 1420–1431. https://doi.org/10.1111/tpj.15389.

[12] Liu H, Zhang MM, Weisz DA, Cheng M, Pakrasi HB, Blankenship RE. Structure of cyanobacterial phycobilisome core revealed by structural modeling and chemical cross-linking. Science Advances. 2021; 7: eaba5743. https://doi.org/10.1126/sciadv.aba5743.

[13] Ajlani G, Vernotte C. Deletion of the PB-loop in the L(CM) subunit does not affect phycobilisome assembly or energy transfer functions in the cyanobacterium *Synechocystis* sp. PCC6714. European Journal of Biochemistry. 1998; 257: 154–159. https://doi.org/10.1046/j.1432-1327.1998.2570154.x.

[14] Wang X, Dong LL, Zhang CX, Zhu KZ, Zhao JQ, Zhao KH, *et al*. Sll1466, a glycosyl transferase homolog involved in global cellular regulation and high-light tolerance of *Synechocystis* PCC6803. Biochemical and Biophysical Research Communications. 2011; 408: 674–679. https://doi.org/10.1016/j.bbrc.2011.04.086.

[15] Porra RJ, Thompson WA, Kriedemann PE. Determination of accurate extinction coefficients and simultaneous equations for assaying chlorophylls a and b extracted with four different solvents: verification of the concentration of chlorophyll standards by atomic absorption spectroscopy. Biochimica et Biophysica Acta (BBA)-Bioenergetics. 1989; 975: 384–394. https://doi.org/10.1016/S0005-2728(89)80347-0.

[16] Bennett A, Bogorad L. Complementary chromatic adaptation in a filamentous blue-green alga. The Journal of Cell Biology. 1973; 58: 419–435. https://doi.org/10.1083/jcb.58.2.419.

[17] Sato H, Fujimori T, Sonoike K. sll1961 is a novel regulator of phycobilisome degradation during nitrogen starvation in the cyanobacterium *Synechocystis* sp. PCC 6803. FEBS Letters. 2008; 582: 1093–1096. https://doi.org/10.1016/j.febslet.2008.02.063.

[18] Sambrook J, Fritsch E, Maniatis T. Molecular cloning: a laboratory manual. 2nd edn. Cold Spring Harbour Laboratory Press: New York. 1989.

[19] Zlenko DV, Elanskaya IV, Lukashev EP, Bolychevtseva YV, Suzina NE, Pojidaeva ES, *et al*. Role of the PB-loop in ApcE and phycobilisome core function in cyanobacterium *Synechocystis* sp. PCC 6803. Biochimica et Biophysica Acta. Bioenergetics. 2019; 1860: 155–166. https://doi.org/10.1016/j.bbabio.2018.10.004.

[20] Golden SS, Brusslan J, Haselkorn R. Genetic engineering of the cyanobacterial chromosome. Methods in Enzymology. 1987; 153: 215–231. https://doi.org/10.1016/0076-6879(87)53055-5.

[21] Gao X, Zhang N, Wei TD, Su HN, Xie BB, Dong CC, *et al*. Crystal structure of the N-terminal domain of linker L(R) and the assembly of cyanobacterial phycobilisome rods. Molecular Microbiology. 2011; 82: 698–705. https://doi.org/10.1111/j.1365-2958.2011.07844.x.

[22] Hu PP, Hou JY, Xu YL, Niu NN, Zhao C, Lu L, *et al*. The role of lyases, NblA and NblB proteins and bilin chromophore transfer in restructuring the cyanobacterial light-harvesting complex‡. The Plant Journal: for Cell and Molecular Biology. 2020; 102: 529–540. https://doi.org/10.1111/tpj.14647.

[23] Glazer AN, Fang S. Chromophore content of blue-green algal phycobiliproteins. The Journal of Biological Chemistry. 1973; 248: 659–662.

[24] Calzadilla PI, Zhan J, Sétif P, Lemaire C, Solymosi D, Battchikova N, *et al*. The Cytochrome b_6f Complex Is Not Involved in Cyanobacterial State Transitions. The Plant Cell. 2019; 31: 911–931. https://doi.org/10.1105/tpc.18.00916.

[25] Shen G, Boussiba S, Vermaas WF. *Synechocystis* sp PCC 6803 strains lacking photosystem I and phycobilisome function. The Plant Cell. 1993; 5: 1853–1863. https://doi.org/10.1105/tpc.5.12.1853.

[26] Wilson A, Ajlani G, Verbavatz JM, Vass I, Kerfeld CA, Kirilovsky D. A soluble carotenoid protein involved in phycobilisome-related energy dissipation in cyanobacteria. The Plant Cell. 2006; 18: 992–1007. https://doi.org/10.1105/tpc.105.040121.

[27] Ma W, Ogawa T, Shen Y, Mi H. Changes in cyclic and respiratory electron transport by the movement of phycobilisomes in the cyanobacterium *Synechocystis* sp. strain PCC 6803. Biochimica et Biophysica Acta. 2007; 1767: 742–749. https://doi.org/10.1016/j.bbabio.2007.01.017.

[28] McConnell MD, Koop R, Vasil'ev S, Bruce D. Regulation of the distribution of chlorophyll and phycobilin-absorbed excitation energy in cyanobacteria. A structure-based model for the light state transition. Plant Physiology. 2002; 130: 1201–1212. https://doi.org/10.1104/pp.009845.

[29] Eilers PHC, Peeters JCH. A model for the relationship between light intensity and the rate of photosynthesis in phytoplankton. Ecological Modelling. 1988; 42: 199–215. https://doi.org/https://doi.org/10.1016/0304-3800(88)90057-9.

[30] Perkins RG, Mouget JL, Lefebvre S, Lavaud J. Light response curve methodology and possible implications in the application of chlorophyll fluorescence to benthic diatoms. Marine Biology. 2006; 149: 703–712. https://doi.org/10.1007/s00227-005-0222-z.

[31] Bradford MM. A rapid and sensitive method for the quantitation of microgram quantities of protein utilizing the principle of protein-dye binding. Analytical Biochemistry. 1976; 72: 248–254. https://doi.org/10.1016/0003-2697(76)90527-3.

[32] Elanskaya IV, Zlenko DV, Lukashev EP, Suzina NE, Kononova IA, Stadnichuk IN. Phycobilisomes from the mutant cyanobacterium *Synechocystis* sp. PCC 6803 missing chromophore domain of ApcE. Biochimica et Biophysica Acta. Bioenergetics. 2018; 1859: 280–291. https://doi.org/10.1016/j.bbabio.2018.01.003.

[33] Laemmli UK. Cleavage of structural proteins during the assembly of the head of bacteriophage T4. Nature. 1970; 227: 680–685. https://doi.org/10.1038/227680a0.

[34] Berkelman TR, Lagarias JC. Visualization of bilin-linked peptides and proteins in polyacrylamide gels. Analytical Biochemistry. 1986; 156: 194–201. https://doi.org/10.1016/0003-2697(86)90173-9.

[35] Jallet D, Gwizdala M, Kirilovsky D. ApcD, ApcF and ApcE are not required for the Orange Carotenoid Protein related phycobilisome fluorescence quenching in the cyanobacterium *Synechocystis* PCC 6803. Biochimica et Biophysica Acta. 2012; 1817: 1418–1427. https://doi.org/10.1016/j.bbabio.2011.11.020.

[36] Mullineaux CW, Allen JF. State 1-State 2 transitions in the cyanobacterium Synechococcus 6301 are controlled by the redox state of electron carriers between Photosystems I and II. Photosynthesis Research. 1990; 23: 297–311. https://doi.org/10.1007/BF00034860.

[37] Goosney D, Miller A. High rates of O2 photoreduction by the unicellular cyanobacterium *Synechocystis* PCC 6803 as determined by the quenching of chlorophyll fluorescence. Canadian Journal of Botany. 2011; 75: 394–401. https://doi.org/10.1139/b97-042.

[38] Levi M, Sendersky E, Schwarz R. Decomposition of cyanobacterial light harvesting complexes: NblA-dependent role of the bilin lyase homolog NblB. The Plant Journal: for Cell and Molecular Biology. 2018; 94: 813–821. https://doi.org/10.1111/tpj.13896.

[39] Baier A, Winkler W, Korte T, Lockau W, Karradt A. Degradation of phycobilisomes in *Synechocystis* sp. PCC6803: evidence for essential formation of an NblA1/NblA2 heterodimer and its codegradation by A Clp protease complex. The Journal of Biological Chemistry. 2014; 289: 11755–11766. https://doi.org/10.1074/jbc.M113.520601.

[40] Glazer AN. Phycobiliproteins — a family of valuable, widely used fluorophores. Journal of Applied Phycology. 1994; 6: 105–112. https://doi.org/10.1007/BF02186064.

[41] Kirilovsky D. Modulating energy arriving at photochemical reaction centers: orange carotenoid protein-related photoprotection and state transitions. Photosynthesis Research. 2015; 126: 3–17. https://doi.org/10.1007/s11120-014-0031-7.

[42] Kaňa R. Mobility of photosynthetic proteins. Photosynthesis Research. 2013; 116: 465–479. https://doi.org/10.1007/s11120-013-9898-y.

[43] Kerfeld CA, Melnicki MR, Sutter M, Dominguez-Martin MA. Structure, function and evolution of the cyanobacterial orange carotenoid protein and its homologs. The New Phytologist. 2017; 215: 937–951. https://doi.org/10.1111/nph.14670.

[44] Büchel C, Wilhelm C. In vivo analysis of slow chlorophyll fluorescence induction kinetics in algae: progress, problems and perspectives. Photochemistry and Photobiology. 1993; 58: 137–148. https://doi.org/10.1111/j.1751-1097.1993.tb04915.x.

[45] Campbell D, Hurry V, Clarke AK, Gustafsson P, Oquist G. Chlorophyll fluorescence analysis of cyanobacterial photosynthesis and acclimation. Microbiology and Molecular Biology Reviews: MMBR. 1998; 62: 667–683. https://doi.org/10.1128/MMBR.62.3.667-683.1998.

[46] Huang C, Yuan X, Zhao J, Bryant DA. Kinetic analyses of state transitions of the cyanobacterium Synechococcus sp. PCC 7002 and its mutant strains impaired in electron transport. Biochimica et Biophysica Acta. 2003; 1607: 121–130. https://doi.org/10.1016/j.bbabio.2003.09.006.

[47] Domínguez-Martín MA, Sauer PV, Kirst H, Sutter M, Bína D, Greber BJ, *et al*. Structures of a phycobilisome in light-harvesting and photoprotected states. Nature. 2022; 609: 835–845. https://doi.org/10.1038/s41586-022-05156-4.

[48] Chang L, Liu X, Li Y, Liu CC, Yang F, Zhao J, *et al*. Structural organization of an intact phycobilisome and its association with photosystem II. Cell Research. 2015; 25: 726–737. https://doi.org/10.1038/cr.2015.59.

[49] Calzadilla PI, Kirilovsky D. Revisiting cyanobacterial state transitions. Photochemical & Photobiological Sciences: Official Journal of the European Photochemistry Association and the European Society for Photobiology. 2020; 19: 585–603. https://doi.org/10.1039/c9pp00451c.

[50] Bolychevtseva YV, Tropin IV, Stadnichuk IN. State 1 and State 2 in Photosynthetic Apparatus of Red Microalgae and Cyanobacteria. Biochemistry. Biokhimiia. 2021; 86: 1181–1191. https://doi.org/10.1134/S0006297921100023.

[51] Muzzopappa F, Wilson A, Kirilovsky D. Interdomain interactions reveal the molecular evolution of the orange carotenoid protein. Nature Plants. 2019; 5: 1076–1086. https://doi.org/10.1038/s41477-019-0514-9.

[52] Sui SF. Structure of Phycobilisomes. Annual Review of Biophysics. 2021; 50: 53–72. https://doi.org/10.1146/annurev-biophys-062920-063657.

[53] Bryant DA, Gisriel CJ. The structural basis for light harvesting in organisms producing phycobiliproteins. The Plant Cell. 2024; 36: 4036–4064. https://doi.org/10.1093/plcell/koae126.